Tuning the cavity modes of a Fabry–Perot resonator using gold nanoparticles

Anirban Mitra,[1] Hayk Harutyunyan,[2] Stefano Palomba,[2] and Lukas Novotny[1,2,*]

[1]*Department of Physics and Astronomy, University of Rochester, Rochester, New York 14627, USA*
[2]*Institute of Optics, University of Rochester, Rochester, New York 14627, USA*
**Corresponding author: novotny@optics.rochester.edu*

Received January 6, 2010; revised February 19, 2010; accepted February 20, 2010;
posted March 2, 2010 (Doc. ID 122197); published March 19, 2010

We study the interaction between a planar Fabry–Perot microcavity and a single embedded gold nanoparticle. We record spatially resolved white-light transmission spectra and show that the interaction between microcavity and nanoparticle gives rise to a redshift of the cavity modes, in accordance with the Bethe–Schwinger cavity perturbation formula. The spectral tuning of cavity modes by discrete nanoparticles can be exploited for applications such as optical and micromechanical sensing. © 2010 Optical Society of America

OCIS codes: 120.2230, 130.3990, 350.4990.

Optical microcavities have found a wide variety of applications in both fundamental and applied fields of research [1], including cavity quantum electrodynamics [2], optical communication [3,4], resonant cavity optoelectronics [5], micromechanical sensors [6], and biosensing [7–9]. The fact that optical microcavities exhibit high-quality factors and small volumes has proven to be extremely useful in highly sensitive applications. Typically, the microcavity needs to be brought into resonance with a target system (e.g., atomic/molecular absorption), but the spectral tuning of microcavities remains a major challenge. Temperature control of refractive indices [10,11] has been pursued in different applications, but the tunability is usually very limited (<1 nm). Larger frequency shifts [12,13] can be achieved with mechanical shape control, but this approach suffers from poor accuracy and irreversible modifications. Electrical tuning is more precise, but again the tunability is limited [14–16]. Hence, the predictable and reliable tuning of an optical microcavity over a reasonably large spectral range remains a challenge.

In this Letter, we demonstrate a method to tune the resonant modes of a Fabry–Perot-type microcavity using gold nanoparticles. The resonance shift observed by a single nanoparticle can be described by Bethe–Schwinger cavity perturbation formula [17,18],

$$\frac{\omega-\omega_m}{\omega_m}=-\frac{\int_V[\mathbf{E}_o^*\epsilon_o\Delta\epsilon(\mathbf{r})\mathbf{E}+\mathbf{H}_o^*\mu_o\Delta\mu(\mathbf{r})\mathbf{H}]dV}{\int_V[\epsilon_o\epsilon(\mathbf{r})\mathbf{E}_o^*\cdot\mathbf{E}+\mu_o\mu(\mathbf{r})\mathbf{H}_o^*\cdot\mathbf{H}]dV}. \tag{1}$$

Here, $\mathbf{E}_o$, $\mathbf{H}_o$ are the unperturbed cavity fields (in absence of the gold nanoparticle) and $\mathbf{E}$, $\mathbf{H}$ are the perturbed cavity fields. V designates the cavity volume, and the electromagnetic properties of the cavity are defined by $\epsilon(\mathbf{r})$ and $\mu(\mathbf{r})$. ω_m is the mth mode resonance frequency in absence of the perturbation, and ω is the resonance in presence of the perturbation. $\Delta\epsilon$ and $\Delta\mu$ denote the properties of the perturbation relative to the unperturbed situation. We assume that the perturbation has a small effect on the cavity and therefore rewrite Eq. (1) as a first-order approximation by using $\mathbf{E}=\mathbf{E}_o$ and $\mathbf{H}=\mathbf{H}_o$.

We consider a planar cavity with reflecting end faces. The area illuminated by the white-light source is A, and the end faces are separated by a distance L. The electric and magnetic fields inside the cavity are calculated to be $E_o\sin[\omega_m z/c]$ and $-i\sqrt{\epsilon_o/\mu_o}E_o\cos[\omega_m z/c]$, respectively. The coordinate z is perpendicular to the surfaces of the end faces. The denominator of Eq. (1) is easily determined to be $V\epsilon_o E_o^2$, where $V=LA$. We place a spherical nanoparticle with volume ΔV inside the cavity and assume that the field is homogeneous across the dimensions of the particle. The perturbation in the dielectric constant is $\Delta\epsilon=\epsilon(\mathbf{r})-\epsilon_p$, with ϵ_p being the dielectric constant of the gold nanoparticle. The nominator of Eq. (1) is calculated to be $\Delta V\Delta\epsilon\epsilon_o E_o^2$, with ΔV being the volume of the perturbation. We then obtain

$$\frac{\lambda-\lambda_m}{\lambda}=\Delta\epsilon\frac{\Delta V}{V}, \tag{2}$$

where we replaced the frequencies ω by corresponding wavelengths λ. Thus, we find that the resonance shift scales with the ratio of the illuminated volume of the microcavity and the perturbation volume (i.e., the volume of the particle).

To fabricate the microcavity, a 40-nm-thick layer of silver is first deposited on a cleaned glass coverslip by e-beam evaporation. A 120 nm polymer layer is then deposited on top of the silver by spin coating 100 μl of a 3.4% Poly(methyl methacrylate) (PMMA, mol. wt. 5000) solution in toluene (purity 99.99%, and hardened by baking at 130°C for 10 min. The PMMA surface is then functionalized by evaporating (3-aminopropyl)trimethoxysilane (APTMES) at 60°C. A dilute solution of 100 nm diameter gold nanoparticles is then spin cast on the surface of the functionalized PMMA. Subsequently, a second layer of PMMA with twice the thickness of the first layer is deposited fol-

lowing the same procedures. Finally, a 40 nm layer of silver is deposited on top of the PMMA. The microcavity hence obtained features spatially separated 100 nm gold nanoparticles embedded in a 340 nm layer of PMMA sandwiched between two reflecting surfaces of silver. The thicknesses of the deposited layers have been verified using atomic force microscopy (AFM) measurements. The fabricated device is schematically shown in Fig. 1 (inset).

Figure 1 illustrates the experimental setup that was used to perform the microcavity detuning experiments. Polychromatic light from a fiber-optic illuminator is coupled into a multimode fiber whose output is collimated using a fiber-optic collimator and focused onto the microcavity by an air objective (50×, 0.8 NA). The transmitted light from the microcavity is collected by an inverted oil objective (100×, 1.3 NA) and directed through a confocal pinhole of diameter 50 μm to a spectrometer, which uses a CCD camera to record transmission spectra. The microcavity is mounted on a scanning stage (resolution 0.1 nm), which allows the microcavity to be translated in the transverse plane. Figure 2(a) shows a representative spectrum of the white-light incident on the cavity.

The piezo stage allows us to raster scan the microcavity and to center individual gold nanoparticles into the light path. Figure 2(b) shows the cavity transmittance spectrum acquired in presence of a single gold nanoparticle [gray (red online)] and absence of any particles [black (blue online)]. The two peaks in the spectrum correspond to the $m=2$ and $m=3$ cavity modes and will be described later. The resonance shift due to the perturbing effect of a single gold nanoparticle is clearly resolved and can be compared with theoretical predictions.

A planar microcavity with partially reflecting end mirrors obeys the resonance condition [19]

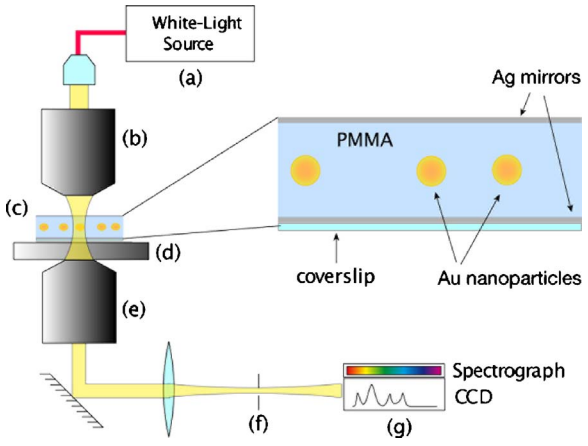

Fig. 1. (Color online) Experimental configuration. White light from a fiber-optic illuminator (a) is coupled into a multimode fiber, collimated and then focused by an air objective (b) onto the microcavity (c). The microcavity is raster-scanned across the focus using a $x-y$ piezo stage (d). The transmitted light from the microcavity is collected by a high-NA oil objective (e) and directed through a confocal imaging pinhole (f) to a spectrometer (g). The inset shows the structural details of the microcavity.

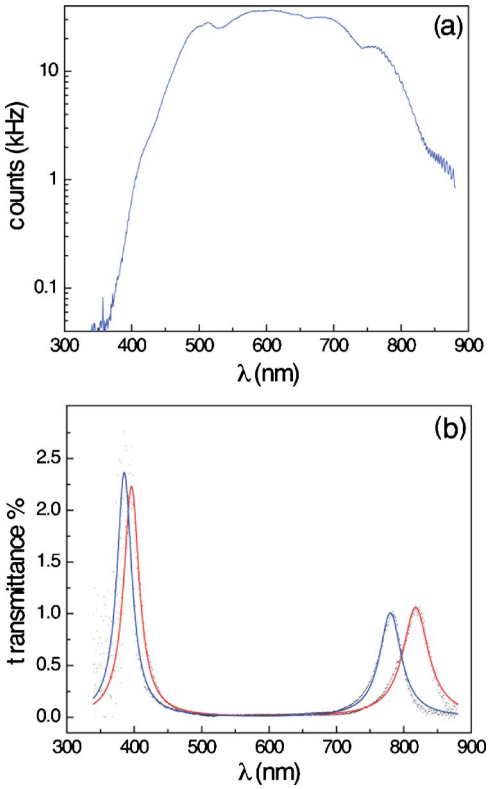

Fig. 2. (Color online) (a) Spectrum of the white-light source employed in the experiments. (b) Cavity transmission spectrum in the absence [black (blue online)] and presence [gray (red online)] of a single gold nanoparticle. The solid lines are Lorentzian fits to the experimental data (black dots).

$$n_{\mathrm{pol}} L \cos\theta = \frac{\lambda}{2}\left[m - \sum_i \Delta\phi_i(d_i,\theta,\lambda)/2\pi\right], \qquad (3)$$

where $m=1,2,3\ldots$ and $i=1,2$. $n_{\mathrm{pol}}=1.4893$ denotes the refractive index of PMMA, L represents the total thickness of the PMMA film, and θ is the angle of incidence of the incident light. m indicates the cavity resonance mode and the index i denotes the upper or lower silver surface. $\Delta\phi_{1,2}$ are the phase changes due to reflection and $d_{1,2}$ are the silver film thicknesses. Because of the weak focusing in our configuration we can approximate the angle of incidence as $\theta\approx 0$.

For $m=1$, the resonance wavelength that satisfies Eq. (3) is outside the spectral range of our white-light source and therefore cannot be observed. However, the peaks of the $m=2$ and $m=3$ cavity modes are clearly resolved in the transmittance spectrum [c.f. Fig. 2(b)]. The $m=2$ resonance peak is at $\lambda_{m=2}=780.12$ nm ($\Delta\phi\approx 2.7$ for $d_{1,2}=40$ nm) [20], and its quality factor is $Q\approx 19$. Using these values in Eq. (3) yields a cavity length of $L=307.1$ nm, which is close to the thickness of ~340 nm measured by AFM. The deviation can be attributed to PMMA thickness variations due to embedded gold nanoparticles. Equation (3) yields a value of $\lambda_{m=3}=387$ nm for the $m=3$ mode, which agrees very well with the resonance peak of $\lambda_{m=3}=385$ nm observed in Fig. 2(b). Thus, our nonideal Fabry–Perot cavity is well described by Eq. (3).

Equation (2) predicts that a single gold nanoparticle will redshift the $m=2$ resonance of the microcavity by ~30–100 nm and the $m=3$ resonance by ~10–20 nm. These values can be compared with the measured shifts of $\Delta\lambda_{m=2}=37$ nm and $\Delta\lambda_{m=3}=11$ nm, as shown in Fig. 2(b). Thus, our experimental observations are in good agreement with theoretical predictions, although the exact matching is difficult because of the simplicity of the theory.

To visualize the resonance shifts induced by single gold nanoparticles we raster scanned the microcavity through the stationary excitation beam and recorded transmittance spectra pixel by pixel. The center frequencies of the $m=2$ and $m=3$ resonance peaks were then determined for each image pixel and used to generate the raster scan images shown in Fig. 3. Individual gold nanoparticles give rise to discrete patterns in the image. Each pattern features a positive image contrast indicating a redshift of the cavity resonances. The discrete patterns are superimposed to a background that reflects nonuniformities of the planar microcavity (variations in thickness and material composition). The patterns from the gold nanoparticles vary slightly in size and intensity because of their different locations in the microcavity and because of particle size variations.

In summary, we fabricated Fabry–Perot microcavities with gold nanoparticles sandwiched between two silver mirrors and found that the cavity modes can be tuned in a wide spectral range. The measured resonance shifts are in good agreement with theoretical predictions based on the Bethe–Schwinger cavity perturbation formula. Nanoparticle-based tuning of cavity modes opens up various possible applications. For example, if the material properties of a given nanoparticle are known one can easily determine the particle size from the shifts in the resonance modes. On the other hand, one can use the resonance shifts to determine the dielectric constant of a nanoparticle of known size and hence its material composition. These capabilities can be further enhanced by fine tuning the fabrication process to obtain resonators with higher Q factors and hence improved resolution.

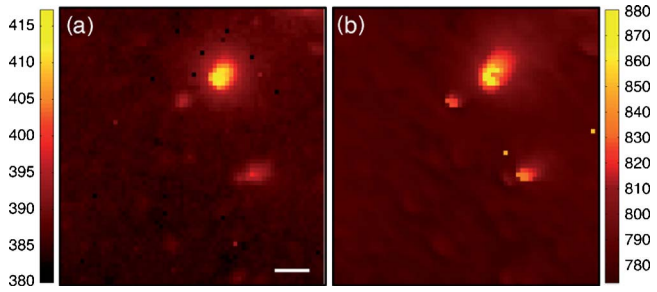

Fig. 3. (Color online) Spatial maps of the center frequencies of $m=2$ and $m=3$ cavity modes. (a) $m=3$ mode, (b) $m=2$ mode. Scalebar: 2 μm.

The authors thank Achim Hartschuh for helpful advice on microcavity fabrication. This work was supported by Agilent Technologies and the National Institutes of Health (NIH) (R21AI085543).

References

1. K. J. Vahala, Nature **424**, 839 (2003).
2. J. P. Reithmaier, G. Sek, A. Löffler, C. Hofmann, S. Kuhn, L. V. K. S. Reitzenstein, V. D. Kulakovskii, T. L. Reinecke, and A. Forchel, Nature **432**, 197 (2004).
3. Y. Hibino, T. Maruno, and K. Okamoto, NTT Tech. Rev. **13**, 4 (2001).
4. S. C. Hagness, D. Rafizadeh, S. T. Ho, and A. Taflove, J. Lightwave Technol. **15**, 2154 (1997).
5. M. S. Ünlü and S. C. Strite, J. Appl. Phys. **78**, 607 (1995).
6. G. Anetsberger, R. Riviere, A. Schlieer, O. Arcizet, and T. Kippenberg, Nat. Photonics **2**, 627 (2008).
7. F. Vollmer and S. Arnold, Nat. Methods **5**, 591 (2008).
8. A. M. Armani, R. P. Kulkarni, S. E. Fraser, R. C. Flagan, and K. J. Vahala, Science **317**, 783 (2007).
9. D. A. Bergstein, E. Ozkumur, A. C. Wu, A. Yalcin, J. Needham, R. Irani, J. Gershoni, B. B. Goldberg, C. DeLisi, M. F. Ruane, and M. S. Ünlü, IEEE J. Sel. Top. Quantum Electron. **14**, 131 (2008).
10. P. Heimala, P. Katila, J. Aarnio, and A. Heinämäki, J. Lightwave Technol. **14**, 2260 (1996).
11. D. Armani, B. Min, A. Martin, and K. J. Vahala, Appl. Phys. Lett. **85**, 5439 (2004).
12. W. von Klitzing, R. Long, V. S. Ilchenko, J. Hare, and V. Lefevre-Seguin, New J. Phys. **3**, 14.1 (2001).
13. A. Kiraz, A. Kurt, and M. A. Dündar, Appl. Phys. Lett. **102**, 093713 (2006).
14. B. Maune, R. Lawson, C. Gunn, A. Scherer, and L. Dalton, Appl. Phys. Lett. **83**, 4689 (2003).
15. T. Wang, C. Chu, and C. Lin, Opt. Lett. **32**, 2777 (2007).
16. M. Humar, M. Ravnik, S. Pajk, and I. Musevic, Nat. Photonics **3**, 595 (2009).
17. J. Schwinger, M.I.T. Radiation Lab. Report (MIT, 1943), Vol. 43-34.
18. W. Hauser, *Introduction to the Principles of Electromagnetism* (Addison-Wesley, 1971).
19. M. Steiner, F. Schleifenbaum, C. Stupperich, A. V. Failla, A. Hartschuh, and A. J. Meixner, ChemPhysChem **6**, 2190 (2005).
20. H. Becker, S. E. Burns, N. Tessler, and R. H. Friend, J. Appl. Phys. **81**, 2825 (1997).